Dynamics of gut microbiome – mediated bile acid metabolism in progression to islet autoimmunity

Santosh Lamichhane[1,10], Partho Sen[1,2,10], Alex M. Dickens[1,3], Marina Amaral Alves[1,4], Taina Härkönen[5], Jarno Honkanen[5], Tommi Vatanen[6,7], Ramnik J. Xavier[7], Tuulia Hyötyläinen[8], Mikael Knip[5,9,*], Matej Orešič[1,2,*]

[1]Turku Bioscience Centre, University of Turku and Åbo Akademi University, FI-20520 Turku, Finland

[2]School of Medical Sciences, Örebro University, 702 81 Örebro, Sweden

[3]Department of Chemistry, University of Turku, 20520 Turku, Finland

[4]Walter Mors Institute of Research on Natural Products, Federal University of Rio de Janeiro, 21941-599 Rio de Janeiro, Brazil

[5]Research Program for Clinical and Molecular Metabolism, Faculty of Medicine, University of Helsinki, Finland

[6]The Liggins Institute, University of Auckland, Auckland, New Zealand

[7]The Broad Institute of MIT and Harvard, Cambridge, MA, USA

[8]School of Science and Technology, Örebro University, Örebro, Sweden

[9]Pediatric Research Center, Children's Hospital, University of Helsinki and Helsinki University Hospital, 00290 Helsinki, Finland

[10]Equal contribution

*Correspondence:

Professor Mikael Knip, M.D., Ph.D., Pediatric Research Center, Children's Hospital, University of Helsinki and Helsinki University Hospital, 00290 Helsinki, Finland. Email: mikael.knip@helsinki.fi

Professor Matej Orešič, Ph.D., Turku Bioscience Centre, University of Turku and Åbo Akademi University, FI-20520 Turku, Finland. Phone: +358 44 972 6094; Email: matej.oresic@utu.fi

Abstract

Previous studies suggest that the human gut microbiome is dysregulated in islet autoimmunity, preceding the clinical onset of type 1 diabetes (T1D). The microbiota of the gut plays an important role in the regulation of bile acid (BA) metabolism. However, not much is known about the regulation of BAs during progression to T1D. Here, we analyzed BAs in a longitudinal series of serum (n= 333) and stool (n= 304) samples, collected at 3, 6, 12, 18, 24 and 36 months of age, from children who developed a single islet autoantibody (P1Ab), multiple islet autoantibodies (P2Ab), and controls (CTRs) who remained autoantibody (AAb) negative during the follow-up. In addition, we analyzed the stool microbiome by shotgun metagenomics in a subgroup of these children (n=111). Factor analysis showed that age had the strongest impact on BA and microbiome profiles. We found that, at an early age, the systemic BA (including taurine and glycine conjugates) and microbial secondary BA pathways were altered in the P2Ab group as compared to the P1Ab or CTR groups. Our findings thus suggest that dysregulated BA metabolism in early life may contribute to the risk and pathogenesis of T1D.

Keywords

Bile acids; genome-scale metabolic modeling; gut microbiome; lipid metabolism; microbial metabolism; islet autoimmunity, type 1 diabetes

Abbreviations

AED: average European diet; AGORA: assembly of gut organisms through reconstruction and analysis; BAs: bile acids; BSH: bile salt hydrolase; CA: cholic acid; CDCA: chenodeoxycholic acid; FSP: faecal secretion potential; EMP: estimated metabolic potential; FXR: farnesoid X receptor; GCA: glycocholic acid; GCDCA: glycochenodeoxycholic acid; GDCA: glycodeoxycholic acid; GEMs: genome-scale metabolic models; GSMM: genome-scale metabolic modeling; HCA: hyocholic acid; MCA: muricholic acids; MS: mass spectrometry; sIECs: small intestinal epithelial cells; TCA: taurocholic acid; TDCA: taurodeoxycholic acid; TGR5: Takeda G protein-coupled membrane receptor 5; THCA: taurohyocholic acid; UDCA: ursodeoxycholic acid: DCA: deoxycholic acid; UPLC-QqQMS: ultra-performance liquid chromatography-tandem mass-spectrometry; VMH: virtual metabolic human database.

Introduction

Bile acids (BAs) are amphiphilic molecules that are crucial physiological agents for facilitating the absorption of lipids in the small intestine. BAs are produced from cholesterol in the liver. Primary BAs such as cholic acid (CA) and chenodeoxycholic acid (CDCA) are conjugated with either glycine or taurine in the hepatocytes (de Aguiar Vallim *et al*, 2013). Gut microbes transform primary BAs to secondary BAs in the intestine (Ramírez-Pérez *et al*, 2017). Most of these BAs are re-absorbed back to the liver, while approximately 5% of the total BA pool is excreted *via* feces. Under normal physiological conditions, a small fraction (about 10%) of the BAs are re-circulated and enter the systemic (enterohepatic) circulation, where they act as ligands for receptors in the peripheral tissues, including farnesoid X receptor (FXR) and the membrane receptor known as Takeda G protein-coupled membrane receptor (TGR5) (Chiang, 2013; Makishima *et al*, 1999; Wang *et al*, 1999). FXR and TGR5 signaling plays a critical role in regulating the systemic lipid, glucose, and energy homeostasis (Jiang *et al*, 2015; Shapiro *et al*, 2018). Dysregulation of systemic BA metabolism has been linked to multiple diseases, including fatty liver disease, cardiovascular disease, and type 2 diabetes (Chan & Wong, 2019; Shapiro *et al.*, 2018; Zheng *et al*, 2021). Thus, the gut-microbiome-BA axis is increasingly recognized as a therapeutic target for treating metabolic and immune disorders (Chan & Wong, 2019; Gu *et al*, 2017; Targher *et al*, 2021).

Previous metabolome and gut microbiome studies suggest that children who progress to islet autoimmunity and type 1 diabetes (T1D) later in life, are characterized by dysregulation of lipid metabolism (Lamichhane *et al*, 2018; Li *et al*, 2020; Oresic *et al*, 2008; Sen *et al*, 2020) and gut microbiota (Kostic *et al*, 2015; Siljander *et al*, 2019; Vatanen *et al*, 2016), suggesting that there is an interplay between host metabolism, the immune system, and the gut microbiome during early T1D pathogenesis. However, our understanding of both microbial and host regulation of BA pathways in the development of islet autoimmunity is still scarce (Kostic *et al.*, 2015).

Herein, we set out to investigate how microbial BA pathways are regulated in children who develop islet autoimmunity. We analyzed BAs and subject-matched microbiome profiles in a prospective series of samples, which included children who developed multiple autoantibodies (P2Ab) during follow-up and are thus at high risk of progression to T1D later in life (Ziegler *et al*, 2013), and those children who developed only one islet autoantibody (P1Ab) but did not progress to T1D during follow-up. We also included control children (CTRs) who remained islet autoantibody (AAb) negative during follow-up.

Results

Prospective study of bile acids and gut microbiome in children at risk for T1D

We analyzed BAs prospectively in subject-matched stool (n= 304) and serum (n= 333) samples from three study groups: P1Ab (n=23), P2Ab (n=13), and CTR (n=38) (**Figure 1**). From each child, we analyzed stool and serum samples at six different time-points corresponding to the ages of 3, 6, 12, 18, 24, and 36 months. A total of 33 BAs, including both primary (glycine/taurine conjugates) and secondary BAs were assayed. Previously-published stool shotgun metagenomics data (whole-genome shotgun sequencing (WGSS)) from a subset of children (n=111 stool samples in total) (Kostic *et al.*, 2015) were included in the study (**Figure1**).

Age-related changes in bile acid and microbiome profiles

In order to determine the contributions of various factors to the BA profiles, multivariable associations were tested for, applying linear models using co-variates including age, sex, and case status (P1Ab, P2Ab, or CTR), taking into account random effects within an individual sample/subject. Age showed the strongest impact (23 stool and 21 serum BAs at $p < 0.05$; **Figure 2A**), while five stool and one serum BA were different across case groups and one stool and four serum BA were different between sexes (**Tables S1** and **S2**). Primary BAs, including cholic acid (CA) and chenodeoxycholic acid (CDCA), were decreased both in stool and in circulation with increasing age (**Figure 2A**). A similar trend was seen for deoxycholic acid (DCA), a secondary BA. Low levels of other secondary BAs (including their taurine and glycine conjugates) were observed during early infancy (3 and 6 months), which steadily increased at/after the first year of life (12 and 18 months) and remained stable at later ages (24 and 36 months) (**Figure 2A**).

Gut microbial profiles follow the dynamic BA trajectories (**Figure 2A-B, Table S3**). Intuitively, age was the strongest factor associated with the composition of the infant gut microbiome (**Figure S1**). Several microbial species, at the strain level, were distinctively associated ($n = 17$, $p < 0.05$) with age (**Figure 2B, Figure S1**); dominated by *Ruminococcus, Alistipes,* and *Eubacterium* species (spp.) which showed an increasing trend with age (**Figure 2D**). However, this did not stabilize at 36 months of age. On the other hand, the abundances of six out of 17 microbes, including *Bifidobacterium breve*, (**Figure 2D**) were initially decreased during 3 to 12 months of infancy and stabilized at 24 and 36 months of age.

Alteration of the gut microbiome impacts bile acid metabolism in progression to islet autoimmunity

Differential analysis showed that 41 microbial strains were altered (analysis of covariance, ANCOVA; Tukey's honest significant differences (HSD), p.adjusted < 0.05) between the study groups (P1Ab and/or P2Ab and/or CTRs), at at least one time-point (**Figure 3A**). Of note, 25 of 41 microbes were known to exhibit BA metabolic pathways annotated by the Assembly of Gut Organisms through Reconstruction and Analysis (AGORA) compendium (Heinken *et al*, 2019; Magnusdottir *et al*, 2017; Noronha *et al*, 2019). Among these, several strains of *Clostridium, Lachnospiraceae, Ruminococcus* and *Alistipes* were predominant and were altered between the P1Ab and P2Ab groups (**Figure 3A**). Lower abundances of *Clostridium and Lachnospiraceae* strains and increased abundances of *Ruminococcus* strains were apparent between P1Ab *vs.* P2Ab at 18 months and/or 24 months of age.

Pairwise metabolic modeling between microbes revealed that most of these microbes exhibit amensal (50%), parasitic (20%) and commensal (15%) relationships for cross-feeding and biotransformation of BAs in the human gut (**Figure S2**)**.** Several strains such as *Roseburia hominis A2-183, Roseburia inulinivorans DSM 16841, Ruminococcus bromii L2-63, Lachnospiraceae bacterium sp. 5_1_63FAA* can only produce secondary BAs, whilst *Anaerostipes hadrus DSM 3319, Bifidobacterium catenulatum DSM 16992, Bifidobacterium coryneforme DSM 20216, Clostridium bartlettii DSM 16795, Clostridium innocuum 2959, Collinsella aerofaciens ATCC 25986, Coprococcus eutactus ATCC 27759, Eggerthella lenta DSM 2243, Erysipelotrichaceae bacterium 5_2_54FAA, Erysipelotrichaceae bacterium sp. 3_1_53, Eubacterium eligens ATCC 27750, Eubacterium hallii DSM 3353* can interact with at least 10 other microbial strains to carry out BA biotransformation (**Figure S2**). Interestingly, *Alistipes spp.* co-exhibited different kinds of microbial interaction, including amensalism, parasitism and commensalism for BA biotransformation (**Figure S2**). The BA pathways exhibited by these microbes include ten different reaction classes that can carry out

deconjugation, dehydrogenation, dehydroxylation and epimerization of BAs in the human gut (**Figures 3B** and **S3**).

Regulation of secondary bile acid pathways before the emergence of islet autoantibodies

In order to understand the interplay between the gut microbiome and BA biotransformation in the progression to islet autoimmunity, we developed personalized community microbiota models for each child. The community microbiota model comprises 25 abundant microbial strains and their BA reactions (**Figure 3A, Figure S3**).

The community microbiota modeling suggested that the total BA reaction abundances were markedly decreased (Tukey's HSD, p.adjusted < 0.05) in the P2Ab *vs.* P1Ab groups at 6 and 12 months of age, *i.e.*, before the median age of seroconversion (**Figure 4A**). Moreover, at this age, the predicted abundances of bile salt hydrolases (BSH) reaction(s) decreased in the P2Ab *vs.* P1Ab group. However, the abundances of these reactions peaked at 24 months of age (post seroconversion) (**Figure 4B**). At this age, several reactions in the alpha/beta dehydroxylation pathway (12-alpha-, 3-alpha-, 7-beta-hydroxysteroid dehydrogenases and cholate ligase) showed decreased abundances in the P2Ab group (*vs.* P1Ab). The abundances of these reactions peaked at 18 months of age (median age of seroconversion). 7-alpha/beta hydroxylation pathways aid in the production of secondary BAs (*e.g.*, DCA, HCA, HDCA and LCA) from primary BAs (*e.g.*, CA and CDCA), respectively (**Figures 3B** and **4B**).

The community modeling also suggested that the total fecal secretion potential (FSP) of secondary BAs was significantly decreased (Tukey's HSD, p.adjusted < 0.05) in P2Ab (*vs*. P1Ab) group at 12 months of age (**Figure 4C**). Taken together, secondary BA production seems to be decreased in the P2Ab group as compared to P1Ab and/or CTR group(s) with the emergence of islet autoantibodies.

Targeted measurements of BAs revealed a decrease in secondary BA levels in progression to islet autoimmunity

Next, we sought to determine specific BA concentration differences between the three study groups in the longitudinal series of stool and serum samples. We detected several differences in BA concentrations between the study groups. In particular, taurine and glycine conjugates of secondary BAs (*e.g.*, GHDCA, GUDCA, TUDCA, THDCA) were decreased in the P2Ab group at 6 and 12 months of age in stool samples, as compared to the CTR or the P1Ab groups (**Figure 5A**). The levels of GLCA, wMCA and LCA were higher in P2Ab than in P1Ab at 18 months of age. No clear differences were seen for the primary BAs, which further suggests that subsequent steps of BA dehydroxylation and secondary BA production were (dys)regulated in the P2Ab group (**Figure 3B**). However, these differences were less pronounced in the serum samples as compared to the stool samples (**Figure 5**). Moreover, there was no persistent longitudinal trend with respect to the differences in BA levels between the groups throughout follow-up, with the exception of TwMCA which was persistently decreased in P2Ab *vs.* P1Ab and CTR groups.

Next, we compared the total stool and serum BA concentrations in the P1Ab and P2Ab groups in samples obtained before and after the appearance of the first islet autoantibody, respectively. Pairwise analysis (paired t-test, $p < 0.05$) revealed that, before the emergence of islet autoantibodies, the total BA pool, both in stool and serum, was lower in the P2Ab group (**Figure 5B-C**).

Association between BAs, gut microbes and their exchange potentials shows unique patterns of regulation in the P2Ab group

At 12 months of age, the UDCA exchange potential of the gut microbiota was positively associated with several species of *Alistipes* and *Eubacterium,* particularly *Eubacterium ventriosum ATCC 27560* (p.adjusted < 0.05). Furthermore, it was positively associated with the GLCA levels (a downstream product) in stool (**Figure 6A)**. At 18 months, the UDCA exchange potentials were strongly associated with *Roseburia hominis A2-183 and Roseburia inulinivorans DSM 16841ı (*p.adjusted < 0.05), whilst inversely associated with the conjugated and/or unconjugated secondary BAs in the stool samples (**Figure 6B)**. *Clostridium bartlettii DSM 16795* was positively associated with the exchange potential of T (DCA) at 12 months, whereas there was an inverse association at 18 months. Several species of *Alistipes* were inversely associated (p.adjusted < 0.05) with TLCA *(*p.adjusted < 0.05) (**Figure 6A-B**).

Discussion

By combining targeted metabolomics and metagenomics data, we show that host-microbial BA co-metabolism is dysregulated in the progression to islet autoimmunity and overt T1D. Our findings suggest that children who progress to multiple islet autoantibodies (P2Ab) during follow-up, and are thus at high risk of developing T1D later in life (Ziegler *et al.*, 2013), have distinct and persistently-altered systemic BA concentrations and species abundances in the gut microbiome, as compared to those children who develop, at most, a single islet autoantibody (P1Ab), or those who remained negative for islet antibodies (CTRs) during the follow-up.

Our results reveal that children who progressed to multiple islet autoantibodies later in life had decreased concentration of conjugated BAs (GHDCA, GUDCA, TUDCA, and THDCA) in early life. In line with this, tauroursodeoxycholic acid (TUDCA), a conjugated secondary BA, was observed to reduce the incidence of diabetes development by improving the glucose utilization and metabolism in the streptozotocin administered C57BL/6 mice (Bronczek *et al*, 2019). Our personalized community metabolic modeling of the gut microbiota identified specific differences in the BA pathways of P2Ab *vs.* P1Ab or CTR groups. Several intermediary reactions of 7-alpha/beta hydroxylation and bile salt hydrolase (BSH) pathways were altered at or before the age of seroconversion. Alteration of relative abundances of BSH levels are associated with the occurrence and development of various diseases in humans (Song *et al*, 2019). Here, we revealed that the activity of BSH may be related to the development of islet autoimmunity and risk of clinical T1D. Furthermore, our results show that in the P2Ab (*vs.* P1Ab) group, reaction abundances of 7-alpha/beta hydroxylation pathway remained lower at 6 and 12 months of age, which gradually increased at later time-points. BSH pathways are key gatekeepers of BA transformation in the gut (Foley *et al*, 2019). We found stool concentration of secondary BAs, particularly UDCA, DCA, HDCA and their glycine and/or taurine conjugates, were downregulated in P2Ab *vs.* P1Ab and/or CTR groups. Decreased fecal secretion potentials (FSPs) of the secondary BAs in the P2Ab group during early life further support the view that a decrease in secondary BA levels at or before the age of seroconversion might occur due to a decrease in the metabolic potential of the microbiota-encoded 7-alpha/beta hydroxylation pathway, which aids in the transformation of secondary BAs.

We also found that BA concentrations are strongly dependent on the age of the children. In agreement with previous findings (Backhed *et al*, 2015; Milani *et al*, 2017), we observed that

the abundances of gut microbes (with the exception of a few strains) gradually increased with the age of the children. Interestingly, many of these microbes are involved in the biotransformation of BAs (Heinken *et al.*, 2019; Magnusdottir *et al.*, 2017). Recently, a study characterized the age-dependent gut microbial and metabolic changes in the murine gastrointestinal tract (van Best *et al*, 2020), where BAs were identified as a major driver for the early maturation of the gut microbiome.

We acknowledge some limitations of our study, such as the relatively small sample size, as well as the effect of a lack of full, systematic understanding of the impact of confounding lifestyle factors (*e.g.* diet) and these factors' relationship with BA host-co-metabolism. Nevertheless, we report BA changes in a longitudinal setting, defining the time-course of changes in BA metabolism with respect to the onset of islet autoimmunity. It is, however, clear that these findings need to be investigated and replicated in other, larger studies and in heterogeneous populations.

In summary, our findings suggest that dysregulated BA metabolism in early life may contribute to the risk and pathogenesis of T1D. BA metabolism may also be an underlying link between the gut microbiome and host (lipid) metabolism during the period preceding seroconversion to positivity for islet autoantibodies and overt T1D.

Methods

Clinical study setting

The DIABIMMUNE study recruited 832 families in Finland (Espoo), Estonia (Tartu), and Russia (Petrozavodsk) with infants carrying HLA alleles that conferred risk for autoimmunity. The subjects involved in the current study were chosen from the subset (n = 74) of international DIABIMMUNE study children who progressed to at least a single AAb (P1Ab, n = 23), who progressed to multiple islet AAb (P2Ab, n = 13), and controls (CTRs, n = 38), *i.e.* the children who remained islet AAb-negative during the follow-up in a longitudinal series of samples collected at 3, 6, 12, 18, 24 and 36 months from each child (Kostic *et al.* 2015). The study groups were matched for HLA-associated diabetes risk, sex, country and period of birth.

This study was conducted according to the guidelines in the Declaration of Helsinki. The Ethics Committee of the Hospital District of Helsinki and Uusimaa approved the study protocol. All families provided written informed consent prior to sample collection.

Quantification of bile acids

The bile acids were measured in serum and fecal sample as described previously (Jäntti *et al*, 2014; Salihović *et al*, 2020). Briefly, 20 µL of serum, or fecal homogenate (prepared by adding 1:20 (m/v) ultrapure water to 50 mg of feces) was filtered through a Ostro Protein Precipitation and Phospholipid Removal 96-well plate (Waters Corporation, Milford, USA), using 100 µL of cold methanol contemning the internal standard mixtures (LCA-d4, TCA-d4, GUDCA-d4, GCA-d4, CA-d4, UDCA-d4, GCDCA-d4, CDCA-d4, DCA-d4, GLCA-d4). The eluent was collected and evaporated to dryness and the residue was re-suspended in 20 µL of a 40:60 MeOH: H2O v/v mixture. The analyses were performed on an ACQUITY HSS T3 (2.1×100 mm, 1.8 µm) column, Waters (Milford), coupled to a triple quadrupole mass spectrometer (Waters Corporation, Milford, USA) with an atmospheric electrospray interface operating in negative ion mode. Separation was performed using gradient elution with 0.1 % formic acid in water (v/v) (A) and 0.1 % formic acid in acetonitrile:methanol (3:1, v/v) (B) at a flow rate of 0.5 mL/ min. Gradient program was 0 min 15 % B, 0-1 min; 30 % B, 1- 16 min; 16-18 min; 70 %

B, 18–23 min 100 % B, and equilibrium time between runs was 7 min. The injection volume was 5 µL and the column was kept at 35 °C. An external calibration with nine calibration points (0.0025–600 ng/mL) was carried out for use in quantitation.

Analysis of islet autoantibodies

Four diabetes-associated autoantibodies were analyzed from each serum sample with specific radiobinding assays: insulin autoantibodies (IAA), glutamic acid decarboxylase antibodies (GADA), islet antigen-2 antibodies (IA-2A), and zinc transporter 8 antibodies (ZnT8A) as described previously (Knip *et al*, 2010). Islet cell antibodies (ICA) were analyzed with immunofluoresence in those subjects who tested positive for at least one of the autoantibodies. The cut-off values were based on the 99th percentile in non-diabetic children and were 2.80 relative units (RUs) for IAA, 5.36 RU for GADA, 0.78 RU for IA-2A and 0.61 RU for ZnT8A.

Taxonomic / phylogenetic profiling and metagenomic analysis

Raw metagenomic sequencing data was retrieved from (https://diabimmune.broadinstitute.org/) (NCBI BioProject ID: PRJNA231909) (Kostic *et al.*, 2015). Stool (n = 111) samples were common between the published metagenomics data (Kostic *et al.*, 2015), and the stool BAs measured in the present study. Metagenomic data form the matched samples (n=111) were considered for further analysis.

As stated in (Kostic *et al.*, 2015), host genome–contaminated reads and low-quality reads are already removed from the raw sequencing data using kneadData v0.4. Taxonomic microbiome profiles were determined using MetaPhlAn2 (Truong *et al*, 2015) using default parameters.

Genome-scale community modeling of human gut microbiota

Previously, genome-scale metabolic modeling (GSMM) using an Assembly of Gut Organisms through Reconstruction and Analysis (AGORA) approach has been used to elucidate the role of gut microbiota in BA biotransformation in humans (Heinken *et al.*, 2019). In addition, it has been used to estimate the metabolic capabilities of gut microbes and related pathways under different biological conditions (Magnusdottir *et al.*, 2017).

We used GSMM to model the dynamics of BA metabolism aided by human gut microbiota under various conditions. In order to reduce the complexity of community modeling, we included genome-scale metabolic models (GEMs) of 25 abundant gut microbes (strains) that have BA metabolic pathways, and were significantly (ANCOVA; Tukey's HSD p.adjusted < 0.05) altered between the study groups (P1Ab, P2Ab and CTRs), at at least one time-point (**Figure 3A**). All the microbial-GEMs obtained were retrieved from the *'AGORA_BA'* compendium (v1.03) (Heinken *et al.*, 2019; Magnusdottir *et al.*, 2017), stored at the Virtual Metabolic Human Database (VMH) (Noronha *et al.*, 2019) and assessed for further analysis.

Next, we developed personalized community models for each individual by contextualizing the community microbiota model with the metagenomic abundances of the microbes estimated for each individual/sample. A detailed protocol for integration of metagenomic abundances into a community microbiota model has been described elsewhere (Baldini *et al*, 2019; Heinken *et al.*, 2019; Magnusdottir *et al.*, 2017). We performed three types of analysis, (1) Modeling the primary growth of the individual microbe based on Average European Diet (AED) (Magnusdottir *et al.*, 2017; Noronha *et al.*, 2019), (2) Microbe-microbe pairing (co-growth) of 25 abundant microbial strains, to determine the joint ability of the microbes for BA biotransformation, and (3) Personalized community modeling at an individual sample level

using metagenomics data. The simulation results were divided for three different study groups (P1Ab, P2Ab and CTRs). GSMM was performed using the COBRA Toolbox (Heirendt *et al*, 2017) and the Microbiome Modeling Toolbox (MMT) (Baldini *et al.*, 2019) deployed in MATLAB *Inc.,* version R2017a.

The 25 abundant microbial-GEMs were coupled into a community microbiota model using the *'joinModelsPairwiseFromList'* function implemented in the MMT (Baldini *et al.*, 2019). A common luminal compartment '[u]' was introduced that enabled metabolite exchanges and cross-feeding between the microbes. The composition of AED was retrieved from (VMH). The intestinal luminal uptake rates were constrained by the dietary fluxes using *'useDiet'* function. The paired models were allowed to exchange conjugated bile acids (BAs), while the uptake of other metabolites was limited. Different types of metabolic interactions were estimated by the *'simulatePairwiseInteractions'* function deployed in MMT with a minimum growth rate difference of 10% between the microbes. Each microbial model (GEM) was allowed to grow on its own, and as a pair under anaerobic conditions. Flux Variability Analysis (FVA) using *'fastFVA'* function was performed to assess maximum and minimum fluxes incurred by the BA reactions in a paired model. The paired models that carried fluxes through the BA exchange reactions were selected and grouped by their genus (**Figure S2**).

Several metabolic reconstruction/models such as Recon3D (Brunk *et al*, 2018), the small intestinal epithelial cells (sIECs) (Sahoo & Thiele, 2013) model, and the VMH database and bibliographic references were mined, and putative BA transporters in the human gut were identified. The BA transporters and exchange reactions were added. Recon3D as a host model was coupled with the community microbiota model using the *'createMultipleSpeciesModel'* function coded in MMT, subsequently the flux coupling constraints were added. A compartment '[b]' for body fluids was introduced. Sanity checks were performed using the COBRA Toolbox. All community microbiota models were able to carry out basic metabolic tasks, including exchange and transport of BAs. The average metabolic reactions and metabolites of a microbiota community model was 15,800 and 13,900 respectively.

The fecal secretion potential (FSP) of a BA reaction is given by $FSP_{ij} = A_i \times v_j$ (eq.1), where 'FSP_{ij}' denotes the estimated potential of 'j^{th}' BA in 'i^{th}' species. A and v represent the relative abundance of a species and absolute flux potential (mmol/gDw/day), respectively (Heinken *et al.*, 2019; Kumar *et al*, 2018). FSP determines the metabolic efficiency of a particular reaction, under a specified condition. The total FSP determines the metabolic capability/potential of the gut microbes in a community to perform a particular task. Likewise, BA reaction abundances in a community model was estimated by the *'calculateReactionAbundance'* function coded in MMT (Heinken *et al.*, 2019; Noronha *et al.*, 2019).

Statistical analysis

The R statistical programming language (v4.0.4) and MATLAB *Inc.,* (vR2017a) was used for data analysis. The *'Heatmap.2'*, *'boxplot'*, *'beanplot'*, '*gplot*', and '*ggplot2*' R libraries / packages were used for data visualization.

Impact of clinical / demographic factors on stool microbiome

The effect of different factors such as age, sex, presence of antibodies, age of T1D onset, duration of breast feeding, HLA-risk class on the microbiome abundances were evaluated for each sample, and the % of explained variance (EV) was estimated. The data were log2-transformed, centered to zero mean and unit variance (autoscaled). The relative contribution

of each factor to the total variance in the dataset was estimated by fitting a linear regression model, where the normalized abundances of the microbes were regressed to the factor of interest, and thereby median marginal coefficients (R^2) were estimated. This analysis was performed using the *'Scater'* package in R (v4.0.4). Age was found to be a confounding factor (>10% EV).

Differential abundant analysis of the microbiome and BAs across multiple conditions

The metagenomic and BA data were log2-transformed. By combining analysis of covariance (ANCOVA) adjusted for 'age' as a covariate, and posthoc Tukey's HSD test (controls for Type I family-wise error rates at $p < 0.05$), we were able to identify differentially abundant microbes (p.adjusted < 0.05) between a paired condition (*e.g.* P2Ab *vs.* CTRs). This analysis was performed by *'aov'* and *'TukeyHSD'* functions deployed in the *'stats'* package (R v4.0.4). Multivariable associations using linear models were performed using 'MaAsLin2' R package (Mallick *et al*, 2021). The locally-weighted regression plot was made using smoothing interpolation function loess available from ggplot2 package in R. Loess regression was performed using *'loess'* function deployed in the *'stats'* package (R v4.0.4).

Bivariate correlation analysis

'RcmdrMisc' package was used to estimate Spearman's correlation between the BA intensities in the stool, community BA exchange reaction potentials, and related microbial abundances. The p-values were adjusted for FDR at (p.adjusted < 0.05). Results are plotted using *'heatmap.2'* function of *'gplots'* package (v.3.0.4).

Acknowledgements

This study was supported by the Academy of Finland postdoctoral grant (No. 323171 to S.L.), the Novo Nordisk Foundation (Grant no. NNF20OC0063971 to T.H. and M.O.), the Academy of Finland Centre of Excellence in Molecular Systems Immunology and Physiology Research 2012-17, No. 250114 to M.K. and M.O.), and the Academy of Finland project grant (No. 333981 to M.O.). Further support was received from the Swedish Research Council (grant no. 2016-05176 to T.H and M.O), Formas (grant no. 2019-00869 to T.H and M.O) and the Medical Research Funds, Helsinki University Hospital (to M.K.).

The authors thank Tuomas Mikael Lindeman and Peppi Raunioniemi (University of Turku) for excellent technical support in bile acid analysis, and to Dr. Aidan McGlinchey (Örebro University) for editing.

Author contributions

Conceptualization (S.L., P.S., M.O.); Data curation (S.L., P.S., M.A.A.); Formal analysis (S.L., P.S.), Funding acquisition (S.L., T.H., M.K., M.O.); Investigation (S.L., P.S., T.H., J.H., M.K., M.O.); Methodology (P.S., A.M.D., M.A.A., T.H., M.O.); Resources (T.V., R.J.X., T.H., M.K.); Supervision (T.-H., M.K., M.O.); Roles/Writing - first draft (S.L., P.S., M.O.); Writing – critical review & editing (all authors).

Data and code availability

Metagenomic sequencing data can be downloaded from

https://diabimmune.broadinstitute.org/diabimmune/ (NCBI BioProject ID: PRJNA231909).

The targeted bile acid metabolomics datasets generated in this study will be submitted to the NIH Common Fund's National Metabolomics Data Repository (NMDR) website, the Metabolomics Workbench (https://www.metabolomicsworkbench.org).

Scripts for GSMM and data analysis can be downloaded from:

https://github.com/parthoBTK/GSMM_T1D.git

Declaration of interests

The authors declare that they have no conflicts of interest.

References

Backhed F, Roswall J, Peng Y, Feng Q, Jia H, Kovatcheva-Datchary P, Li Y, Xia Y, Xie H, Zhong H *et al* (2015) Dynamics and Stabilization of the Human Gut Microbiome during the First Year of Life. *Cell Host Microbe* 17: 852

Baldini F, Heinken A, Heirendt L, Magnusdottir S, Fleming RMT, Thiele I (2019) The Microbiome Modeling Toolbox: from microbial interactions to personalized microbial communities. *Bioinformatics* 35: 2332-2334

Bronczek GA, Vettorazzi JF, Soares GM, Kurauti MA, Santos C, Bonfim MF, Carneiro EM, Balbo SL, Boschero AC, Costa Junior JM (2019) The Bile Acid TUDCA Improves Beta-Cell Mass and Reduces Insulin Degradation in Mice With Early-Stage of Type-1 Diabetes. *Front Physiol* 10: 561

Brunk E, Sahoo S, Zielinski DC, Altunkaya A, Drager A, Mih N, Gatto F, Nilsson A, Preciat Gonzalez GA, Aurich MK *et al* (2018) Recon3D enables a three-dimensional view of gene variation in human metabolism. *Nat Biotechnol* 36: 272-281

Chan WK, Wong VW (2019) A new bile acid treatment for non-alcoholic fatty liver disease. *Lancet Gastroenterol Hepatol* 4: 747-749

Chiang JY (2013) Bile acid metabolism and signaling. *Compr Physiol* 3: 1191-1212

de Aguiar Vallim TQ, Tarling EJ, Edwards PA (2013) Pleiotropic roles of bile acids in metabolism. *Cell Metab* 17: 657-669

Foley MH, O'Flaherty S, Barrangou R, Theriot CM (2019) Bile salt hydrolases: Gatekeepers of bile acid metabolism and host-microbiome crosstalk in the gastrointestinal tract. *PLoS pathogens* 15: e1007581

Gu Y, Wang X, Li J, Zhang Y, Zhong H, Liu R, Zhang D, Feng Q, Xie X, Hong J *et al* (2017) Analyses of gut microbiota and plasma bile acids enable stratification of patients for antidiabetic treatment. *Nat Commun* 8: 1785

Heinken A, Ravcheev DA, Baldini F, Heirendt L, Fleming RMT, Thiele I (2019) Systematic assessment of secondary bile acid metabolism in gut microbes reveals distinct metabolic capabilities in inflammatory bowel disease. *Microbiome* 7: 75

Heirendt L, Arreckx S, Pfau T, Mendoza SN, Richelle A, Heinken A, Haraldsdottir HS, Keating SM, Vlasov V, Wachowiak J (2017) Creation and analysis of biochemical constraint-based models: the COBRA Toolbox v3. 0. *arXiv preprint arXiv:171004038*

Jäntti SE, Kivilompolo M, Ohrnberg L, Pietiläinen KH, Nygren H, Orešič M, Hyötyläinen T (2014) Quantitative profiling of bile acids in blood, adipose tissue, intestine, and gall bladder

samples using ultra high performance liquid chromatography-tandem mass spectrometry. *Analytical and bioanalytical chemistry* 406: 7799-7815

Jiang C, Xie C, Lv Y, Li J, Krausz KW, Shi J, Brocker CN, Desai D, Amin SG, Bisson WH *et al* (2015) Intestine-selective farnesoid X receptor inhibition improves obesity-related metabolic dysfunction. *Nat Commun* 6: 10166

Knip M, Virtanen SM, Seppä K, Ilonen J, Savilahti E, Vaarala O, Reunanen A, Teramo K, Hämäläinen AM, Paronen J *et al* (2010) Dietary intervention in infancy and later signs of beta-cell autoimmunity. *The New England journal of medicine* 363: 1900-1908

Kostic AD, Gevers D, Siljander H, Vatanen T, Hyotylainen T, Hamalainen AM, Peet A, Tillmann V, Poho P, Mattila I *et al* (2015) The dynamics of the human infant gut microbiome in development and in progression toward type 1 diabetes. *Cell Host Microbe* 17: 260-273

Kumar M, Ji B, Babaei P, Das P, Lappa D, Ramakrishnan G, Fox TE, Haque R, Petri WA, Backhed F *et al* (2018) Gut microbiota dysbiosis is associated with malnutrition and reduced plasma amino acid levels: Lessons from genome-scale metabolic modeling. *Metab Eng* 49: 128-142

Lamichhane S, Ahonen L, Dyrlund TS, Siljander H, Hyöty H, Ilonen J, Toppari J, Veijola R, Hyötyläinen T, Knip M (2018) A longitudinal plasma lipidomics dataset from children who developed islet autoimmunity and type 1 diabetes. *Scientific data* 5: 1-9

Li Q, Parikh H, Butterworth MD, Lernmark A, Hagopian W, Rewers M, She JX, Toppari J, Ziegler AG, Akolkar B *et al* (2020) Longitudinal Metabolome-Wide Signals Prior to the Appearance of a First Islet Autoantibody in Children Participating in the TEDDY Study. *Diabetes* 69: 465-476

Magnusdottir S, Heinken A, Kutt L, Ravcheev DA, Bauer E, Noronha A, Greenhalgh K, Jager C, Baginska J, Wilmes P *et al* (2017) Generation of genome-scale metabolic reconstructions for 773 members of the human gut microbiota. *Nat Biotechnol* 35: 81-89

Makishima M, Okamoto AY, Repa JJ, Tu H, Learned RM, Luk A, Hull MV, Lustig KD, Mangelsdorf DJ, Shan B (1999) Identification of a nuclear receptor for bile acids. *Science* 284: 1362-1365

Mallick H, Rahnavard A, McIver LJ, Ma S, Zhang Y, Nguyen LH, Tickle TL, Weingart G, Ren B, Schwager EH *et al* (2021) Multivariable Association Discovery in Population-scale Meta-omics Studies. *bioRxiv*: 2021.2001.2020.427420

Milani C, Duranti S, Bottacini F, Casey E, Turroni F, Mahony J, Belzer C, Delgado Palacio S, Arboleya Montes S, Mancabelli L *et al* (2017) The First Microbial Colonizers of the Human Gut: Composition, Activities, and Health Implications of the Infant Gut Microbiota. *Microbiol Mol Biol Rev* 81

Noronha A, Modamio J, Jarosz Y, Guerard E, Sompairac N, Preciat G, Danielsdottir AD, Krecke M, Merten D, Haraldsdottir HS *et al* (2019) The Virtual Metabolic Human database: integrating human and gut microbiome metabolism with nutrition and disease. *Nucleic Acids Res* 47: D614-D624

Oresic M, Simell S, Sysi-Aho M, Nanto-Salonen K, Seppanen-Laakso T, Parikka V, Katajamaa M, Hekkala A, Mattila I, Keskinen P *et al* (2008) Dysregulation of lipid and amino acid metabolism precedes islet autoimmunity in children who later progress to type 1 diabetes. *J Exp Med* 205: 2975-2984

Ramírez-Pérez O, Cruz-Ramón V, Chinchilla-López P, Méndez-Sánchez N (2017) The Role of the Gut Microbiota in Bile Acid Metabolism. *Ann Hepatol* 16: s15-s20

Sahoo S, Thiele I (2013) Predicting the impact of diet and enzymopathies on human small intestinal epithelial cells. *Hum Mol Genet* 22: 2705-2722

Salihović S, Dickens AM, Schoultz I, Fart F, Sinisalu L, Lindeman T, Halfvarson J, Orešič M, Hyötyläinen T (2020) Simultaneous determination of perfluoroalkyl substances and bile acids in human serum using ultra-high-performance liquid chromatography-tandem mass spectrometry. *Analytical and bioanalytical chemistry* 412: 2251-2259

Sen P, Dickens AM, Lopez-Bascon MA, Lindeman T, Kemppainen E, Lamichhane S, Ronkko T, Ilonen J, Toppari J, Veijola R *et al* (2020) Metabolic alterations in immune cells associate with progression to type 1 diabetes. *Diabetologia* 63: 1017-1031

Shapiro H, Kolodziejczyk AA, Halstuch D, Elinav E (2018) Bile acids in glucose metabolism in health and disease. *J Exp Med* 215: 383-396

Siljander H, Honkanen J, Knip M (2019) Microbiome and type 1 diabetes. *EBioMedicine* 46: 512-521

Song Z, Cai Y, Lao X, Wang X, Lin X, Cui Y, Kalavagunta PK, Liao J, Jin L, Shang J *et al* (2019) Taxonomic profiling and populational patterns of bacterial bile salt hydrolase (BSH) genes based on worldwide human gut microbiome. *Microbiome* 7: 9

Targher G, Corey KE, Byrne CD, Roden M (2021) The complex link between NAFLD and type 2 diabetes mellitus - mechanisms and treatments. *Nat Rev Gastroenterol Hepatol*

Truong DT, Franzosa EA, Tickle TL, Scholz M, Weingart G, Pasolli E, Tett A, Huttenhower C, Segata N (2015) MetaPhlAn2 for enhanced metagenomic taxonomic profiling. *Nat Methods* 12: 902-903

van Best N, Rolle-Kampczyk U, Schaap FG, Basic M, Olde Damink SWM, Bleich A, Savelkoul PHM, von Bergen M, Penders J, Hornef MW (2020) Bile acids drive the newborn's gut microbiota maturation. *Nat Commun* 11: 3692

Vatanen T, Kostic AD, d'Hennezel E, Siljander H, Franzosa EA, Yassour M, Kolde R, Vlamakis H, Arthur TD, Hamalainen AM *et al* (2016) Variation in Microbiome LPS Immunogenicity Contributes to Autoimmunity in Humans. *Cell* 165: 842-853

Wang H, Chen J, Hollister K, Sowers LC, Forman BM (1999) Endogenous bile acids are ligands for the nuclear receptor FXR/BAR. *Mol Cell* 3: 543-553

Zheng X, Chen T, Zhao A, Ning Z, Kuang J, Wang S, You Y, Bao Y, Ma X, Yu H *et al* (2021) Hyocholic acid species as novel biomarkers for metabolic disorders. *Nat Commun* 12: 1487

Ziegler AG, Rewers M, Simell O, Simell T, Lempainen J, Steck A, Winkler C, Ilonen J, Veijola R, Knip M *et al* (2013) Seroconversion to multiple islet autoantibodies and risk of progression to diabetes in children. *JAMA* 309: 2473-2479

Figure legends

Figure 1. Outlines of analytical study flow. This illustrates the number of serum and stool samples collected for targeted BA measurement at each time-point. The samples were stratified into P1Ab, P2Ab and CTR groups. Moreover, this shows the age at seroconversion among the children taking part in this study.

Figure 2. Age-related changes in the bile acid and microbiome. (A) The loess curve plot of BAs over time (3, 6, 12, 18, and 24) between stool and serum samples. This panel plots, separately, representative primary, secondary and conjugated BAs that changed significantly over time ($p < 0.05$). **(B)** Bar plots showing correlation coefficients for the association between age and different microbes. Red represents inverse correlations while blue represents positive correlations as obtained by multivariate linear regression using MaAsLin2 R package. **(C-D)** The loess curve plot of selected microbes over time.

Figure 3. Microbial strains in progression to islet autoimmunity. **(A)** A heatmap showing the log2 fold changes (FCs) in the strain-level abundances of the gut microbes in P1Ab *vs*. CTRs, P2Ab *vs*. CTRs and P2Ab *vs*. P1Ab groups at 6, 12, 18, 24 and 36 months of the follow-up. Red, blue and yellow color denotes increase, decrease and no change in the abundances between the differential conditions, respectively. Statistical significance was assessed by ANCOVA adjusted for 'age' as a covariate, and Tukey's HSD (p.adjusted < 0.05). Microbes with BA pathways (annotated by the AGORA compendium) are marked with light blue color. **(B)** An illustration of BA metabolism and related pathways in the humans.

Figure 4. Regulation of bile acid reactions in progression to islet autoimmunity. (A,C) Beanplots showing the levels of total BA reaction abundances and the total fecal secretion potentials (FSPs) predicted by the community microbiota models in CTRs, P1Ab and P2Ab groups at 6, 12, 18, 24 and 36 months of the follow-up. The black dotted line denotes the mean of the population. The black dashes in the bean plots represent the group mean. '*' denotes significant differences (ANCOVA + Tukey's HSD, p.adjusted < 0.05). **(B)** Locally Weighted Scatterplot Smoothing (LOWESS) plot showing the longitudinal trend of an individual BA reaction abundance in the CTRs (light blue), P1Ab (yellow) and P2Ab (orange) groups during the follow-up. The shaded area around the curves depicts the 95% confidence interval.

Figure 5. Systemic alterations in bile acid profiles in progression to islet autoimmunity.

(**A)** A heatmap showing the log2 fold changes (FCs) in BA profiles in P1Ab *vs*. CTRs, P2Ab *vs*. CTRs and P2Ab *vs*. P1Ab groups at 6, 12, 18, 24 and 36 months of follow-up. Red, blue and yellow color denotes increase, decrease and no change in the intensities of BAs between the differential conditions, respectively. Statistical significance was estimated by ANCOVA adjusted for 'age' as a covariate, and Tukey's HSD (p.adjusted < 0.05). **(B-C)** Boxplot showing the total intensities of BAs before and after seroconversion in P1Ab and P2Ab groups. Statistical significance was estimated by a paired t-test ($p < 0.1$).

Figure 6. Cross-correlation between the gut microbiome, BA exchange potentials and their systemic (stool) levels in progression to islet autoimmunity.

Correlation plots showing bivariate Spearman's correlations between the gut microbiome (metagenomics) and/or BA exchange potential (microbiota community model) and/or level of BA (lipidomics) in the stool samples of P2Ab (n=111) group at 12 and 18 months. Red, blue

and white/yellow color represents positive, negative and no correlation respectively. The white ‘dot’ depicts that the correlation is statistically significant (p.adjusted < 0.05).

Figure 1

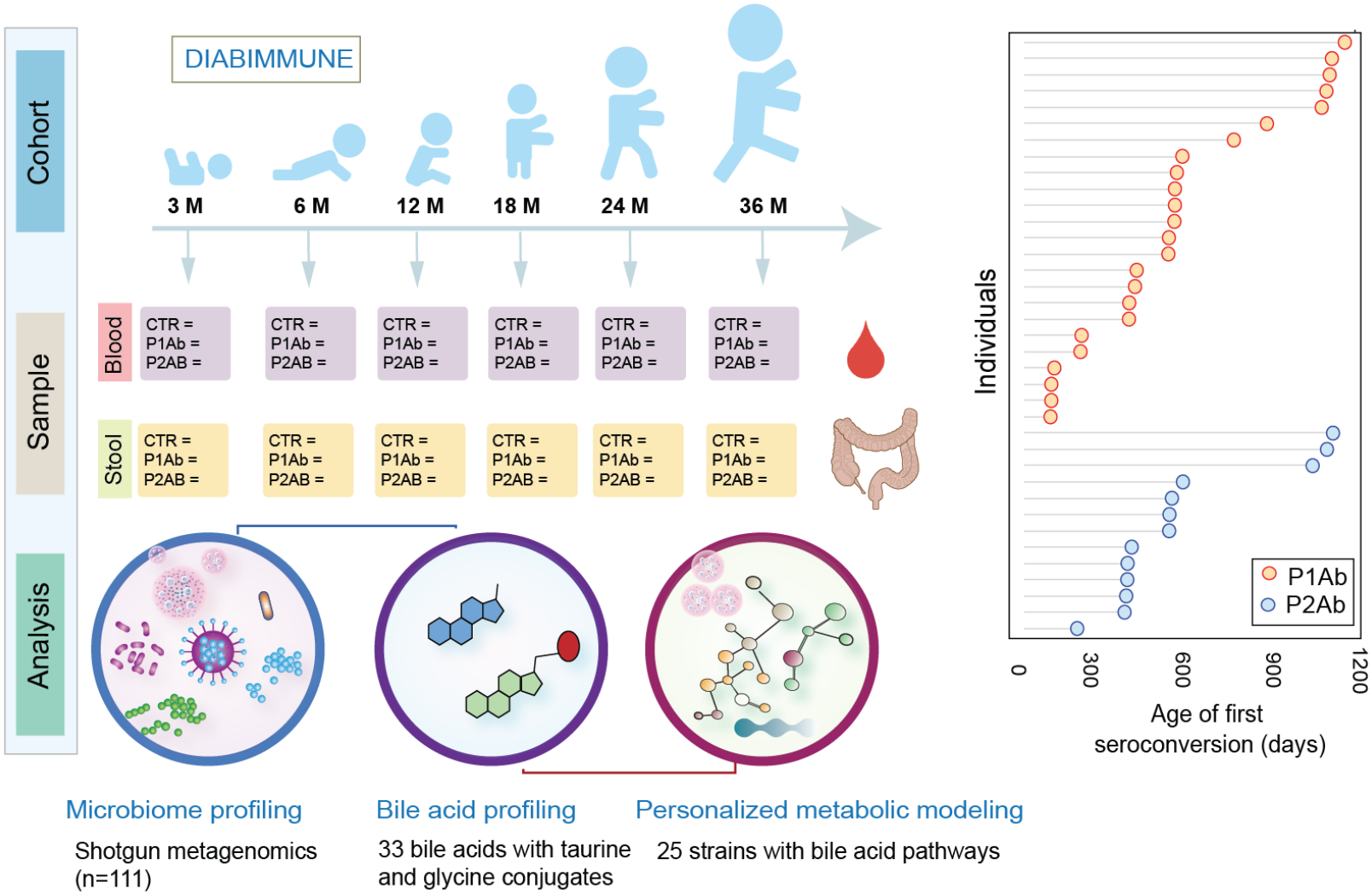
Cohort
Sample
Analysis
DIABIMMUNE
3 M
6 M
12 M
18 M
24 M
36 M
Blood
Stool
CTR =
P1Ab =
P2AB =
Individuals
Age of first seroconversion (days)
0
300
600
900
1200
P1Ab
P2Ab
Microbiome profiling
Shotgun metagenomics (n=111)
Bile acid profiling
33 bile acids with taurine and glycine conjugates
Personalized metabolic modeling
25 strains with bile acid pathways

Figure 2

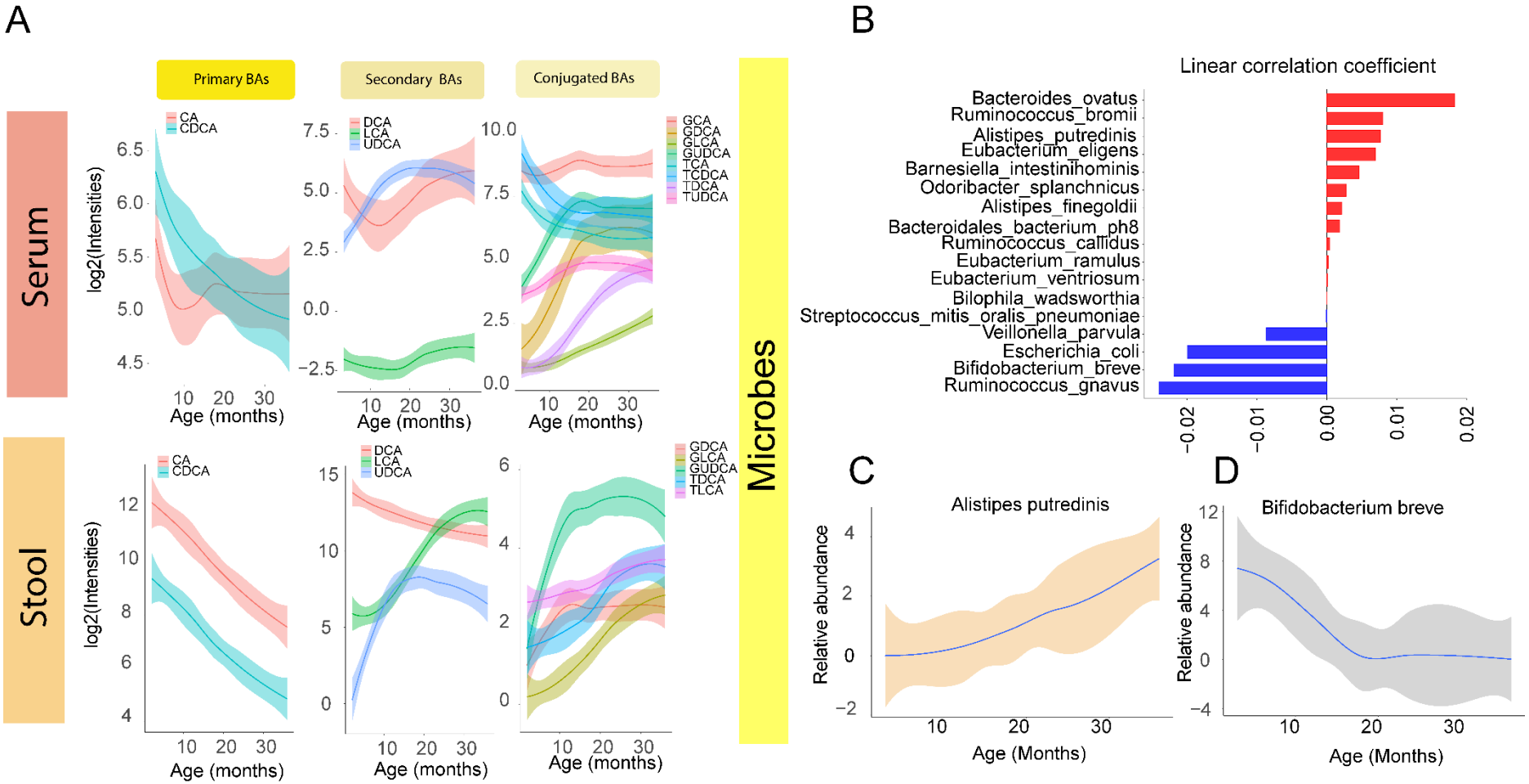
A
Primary BAs
Secondary BAs
Conjugated BAs
Serum
Stool
Microbes
log2(Intensities)
Age (months)
CA
CDCA
DCA
LCA
UDCA
GCA
GDCA
GLCA
GUDCA
TCA
TCDCA
TDCA
TUDCA
TLCA
B
Linear correlation coefficient
Bacteroides_ovatus
Ruminococcus_bromii
Alistipes_putredinis
Eubacterium_eligens
Barnesiella_intestinihominis
Odoribacter_splanchnicus
Alistipes_finegoldii
Bacteroidales_bacterium_ph8
Ruminococcus_callidus
Eubacterium_ramulus
Eubacterium_ventriosum
Bilophila_wadsworthia
Streptococcus_mitis_oralis_pneumoniae
Veillonella_parvula
Escherichia_coli
Bifidobacterium_breve
Ruminococcus_gnavus
C
Alistipes putredinis
D
Bifidobacterium breve
Relative abundance
Age (Months)

Figure 3

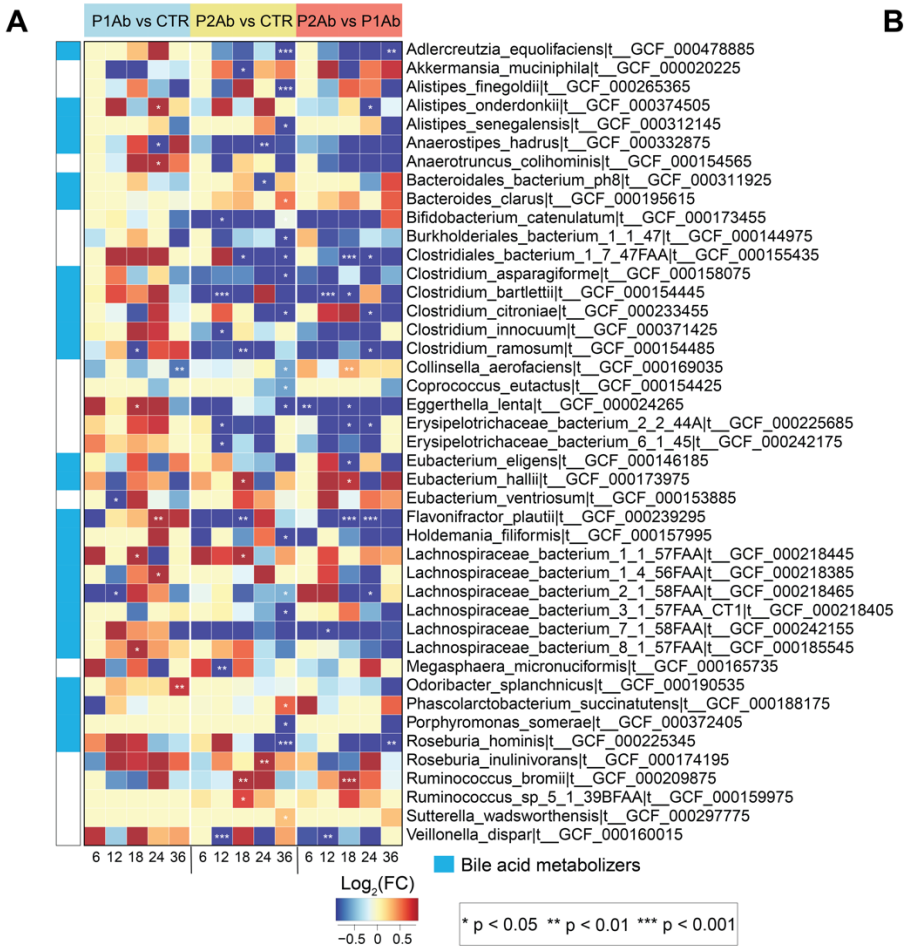
A
P1Ab vs CTR
P2Ab vs CTR
P2Ab vs P1Ab
Adlercreutzia_equolifaciens|t__GCF_000478885
Akkermansia_muciniphila|t__GCF_000020225
Alistipes_finegoldii|t__GCF_000265365
Alistipes_onderdonkii|t__GCF_000374505
Alistipes_senegalensis|t__GCF_000312145
Anaerostipes_hadrus|t__GCF_000332875
Anaerotruncus_colihominis|t__GCF_000154565
Bacteroidales_bacterium_ph8|t__GCF_000311925
Bacteroides_clarus|t__GCF_000195615
Bifidobacterium_catenulatum|t__GCF_000173455
Burkholderiales_bacterium_1_1_47|t__GCF_000144975
Clostridiales_bacterium_1_7_47FAA|t__GCF_000155435
Clostridium_asparagiforme|t__GCF_000158075
Clostridium_bartlettii|t__GCF_000154445
Clostridium_citroniae|t__GCF_000233455
Clostridium_innocuum|t__GCF_000371425
Clostridium_ramosum|t__GCF_000154485
Collinsella_aerofaciens|t__GCF_000169035
Coprococcus_eutactus|t__GCF_000154425
Eggerthella_lenta|t__GCF_000024265
Erysipelotrichaceae_bacterium_2_2_44A|t__GCF_000225685
Erysipelotrichaceae_bacterium_6_1_45|t__GCF_000242175
Eubacterium_eligens|t__GCF_000146185
Eubacterium_hallii|t__GCF_000173975
Eubacterium_ventriosum|t__GCF_000153885
Flavonifractor_plautii|t__GCF_000239295
Holdemania_filiformis|t__GCF_000157995
Lachnospiraceae_bacterium_1_1_57FAA|t__GCF_000218445
Lachnospiraceae_bacterium_1_4_56FAA|t__GCF_000218385
Lachnospiraceae_bacterium_2_1_58FAA|t__GCF_000218465
Lachnospiraceae_bacterium_3_1_57FAA_CT1|t__GCF_000218405
Lachnospiraceae_bacterium_7_1_58FAA|t__GCF_000242155
Lachnospiraceae_bacterium_8_1_57FAA|t__GCF_000185545
Megasphaera_micronuciformis|t__GCF_000165735
Odoribacter_splanchnicus|t__GCF_000190535
Phascolarctobacterium_succinatutens|t__GCF_000188175
Porphyromonas_somerae|t__GCF_000372405
Roseburia_hominis|t__GCF_000225345
Roseburia_inulinivorans|t__GCF_000174195
Ruminococcus_bromii|t__GCF_000209875
Ruminococcus_sp_5_1_39BFAA|t__GCF_000159975
Sutterella_wadsworthensis|t__GCF_000297775
Veillonella_dispar|t__GCF_000160015
6 12 18 24 36
6 12 18 24 36
6 12 18 24 36
Bile acid metabolizers
Log2(FC)
−0.5 0 0.5
* p < 0.05 ** p < 0.01 *** p < 0.001

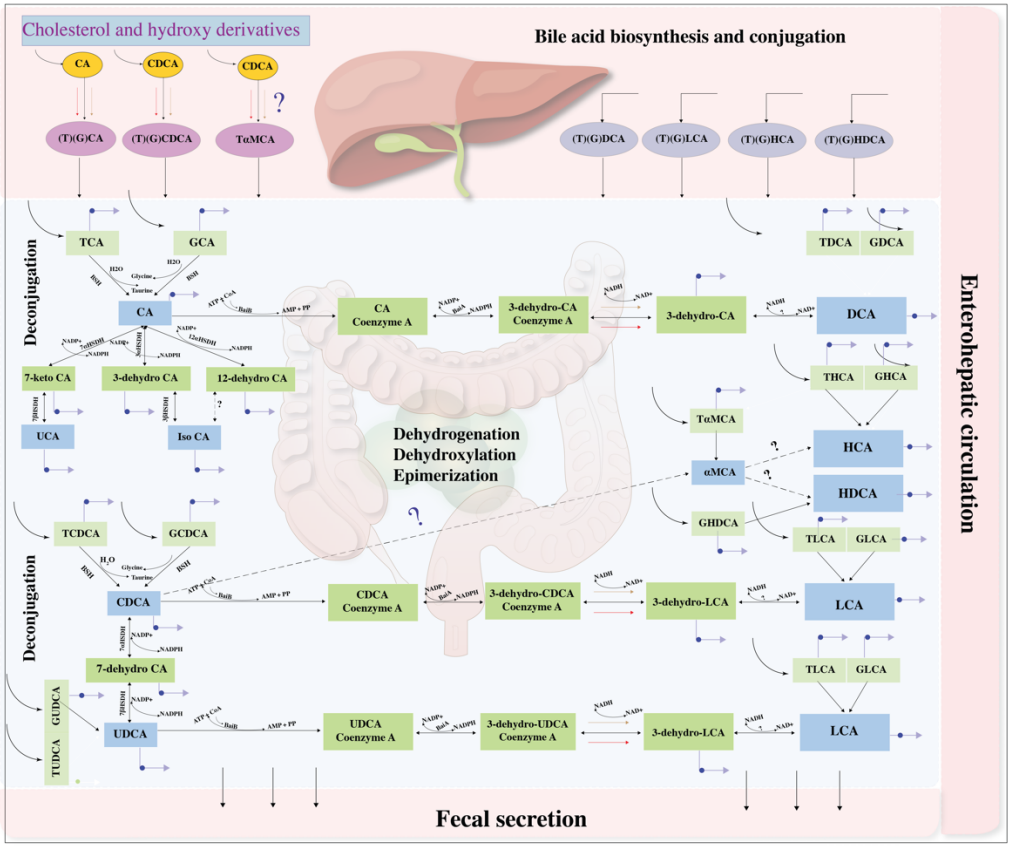
B
Cholesterol and hydroxy derivatives
Bile acid biosynthesis and conjugation
CA
CDCA
CDCA
(T)(G)CA
(T)(G)CDCA
TαMCA
(T)(G)DCA
(T)(G)LCA
(T)(G)HCA
(T)(G)HDCA
Deconjugation
TCA
GCA
TDCA
GDCA
CA
CA Coenzyme A
3-dehydro-CA Coenzyme A
3-dehydro-CA
DCA
7-keto CA
3-dehydro CA
12-dehydro CA
THCA
GHCA
UCA
Iso CA
TαMCA
αMCA
HCA
HDCA
GHDCA
Dehydrogenation
Dehydroxylation
Epimerization
TCDCA
GCDCA
TLCA
GLCA
CDCA
CDCA Coenzyme A
3-dehydro-CDCA Coenzyme A
3-dehydro-LCA
LCA
7-dehydro CA
TLCA
GLCA
GUDCA
TUDCA
UDCA
UDCA Coenzyme A
3-dehydro-UDCA Coenzyme A
3-dehydro-LCA
LCA
Fecal secretion
Enterohepatic circulation

Figure 4

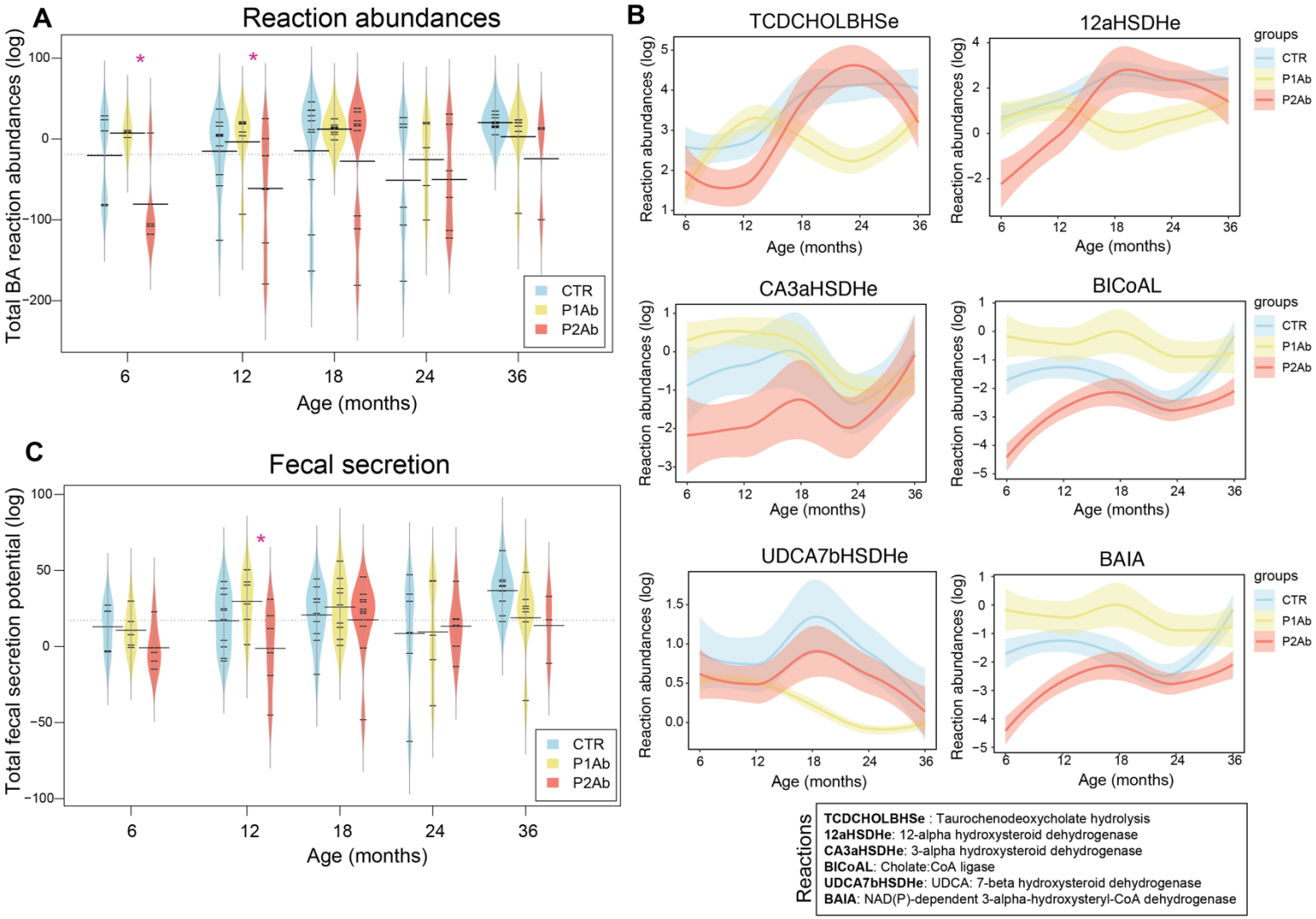
A
Reaction abundances
Total BA reaction abundances (log)
Age (months)
CTR
P1Ab
P2Ab
B
TCDCHOLBHSe
12aHSDHe
CA3aHSDHe
BICoAL
UDCA7bHSDHe
BAIA
Reaction abundances (log)
Age (months)
groups
C
Fecal secretion
Total fecal secretion potential (log)
Reactions
TCDCHOLBHSe : Taurochenodeoxycholate hydrolysis
12aHSDHe: 12-alpha hydroxysteroid dehydrogenase
CA3aHSDHe: 3-alpha hydroxysteroid dehydrogenase
BICoAL: Cholate:CoA ligase
UDCA7bHSDHe: UDCA: 7-beta hydroxysteroid dehydrogenase
BAIA: NAD(P)-dependent 3-alpha-hydroxysteryl-CoA dehydrogenase

Figure 5

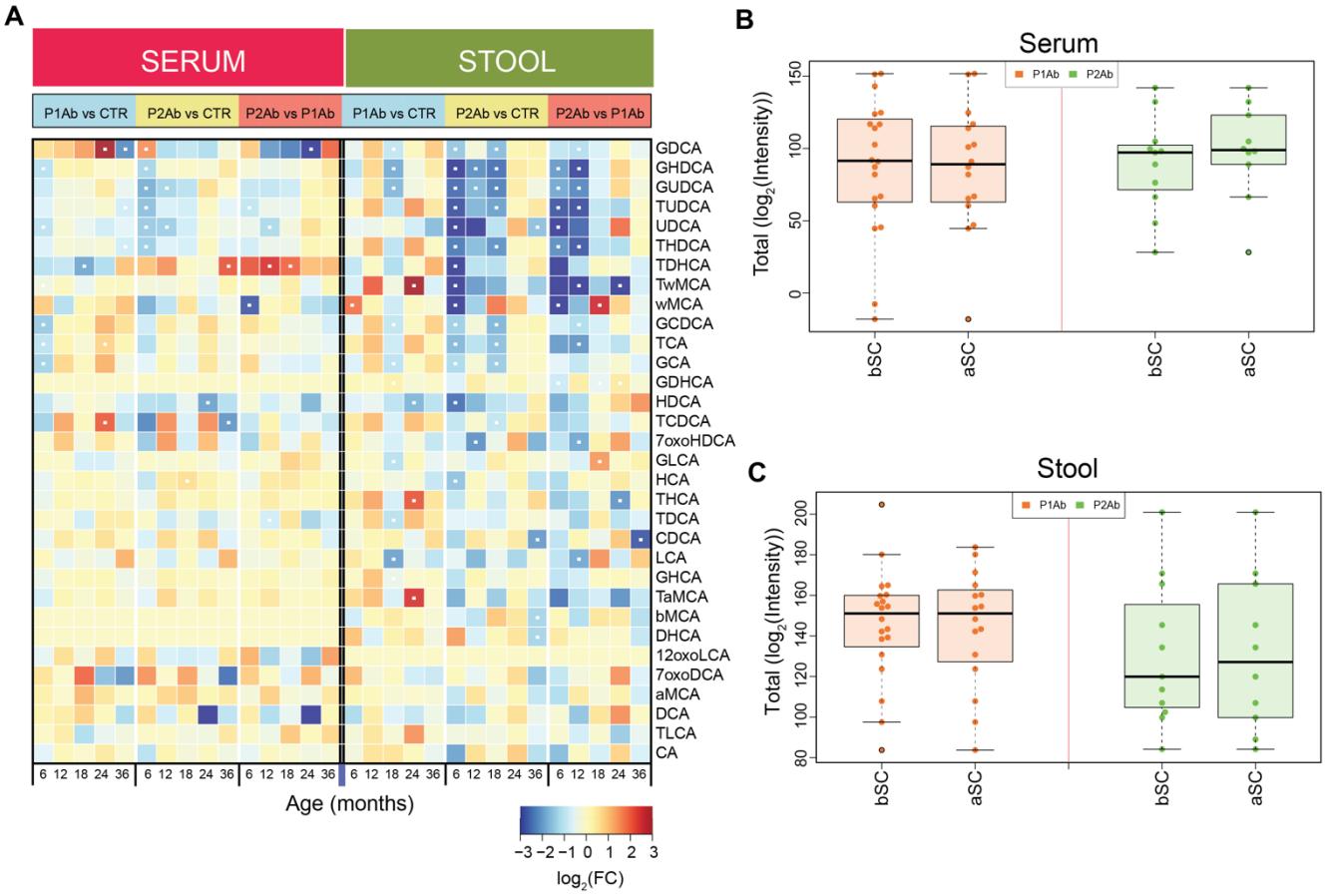
A
SERUM
STOOL
P1Ab vs CTR
P2Ab vs CTR
P2Ab vs P1Ab
P1Ab vs CTR
P2Ab vs CTR
P2Ab vs P1Ab
GDCA
GHDCA
GUDCA
TUDCA
UDCA
THDCA
TDHCA
TwMCA
wMCA
GCDCA
TCA
GCA
GDHCA
HDCA
TCDCA
7oxoHDCA
GLCA
HCA
THCA
TDCA
CDCA
LCA
GHCA
TaMCA
bMCA
DHCA
12oxoLCA
7oxoDCA
aMCA
DCA
TLCA
CA
6 12 18 24 36
Age (months)
−3 −2 −1 0 1 2 3
log2(FC)
B
Serum
P1Ab
P2Ab
Total (log2(Intensity))
0
50
100
150
bSC
aSC
bSC
aSC
C
Stool
P1Ab
P2Ab
Total (log2(Intensity))
80
100
120
140
160
180
200
bSC
aSC
bSC
aSC

Figure 6

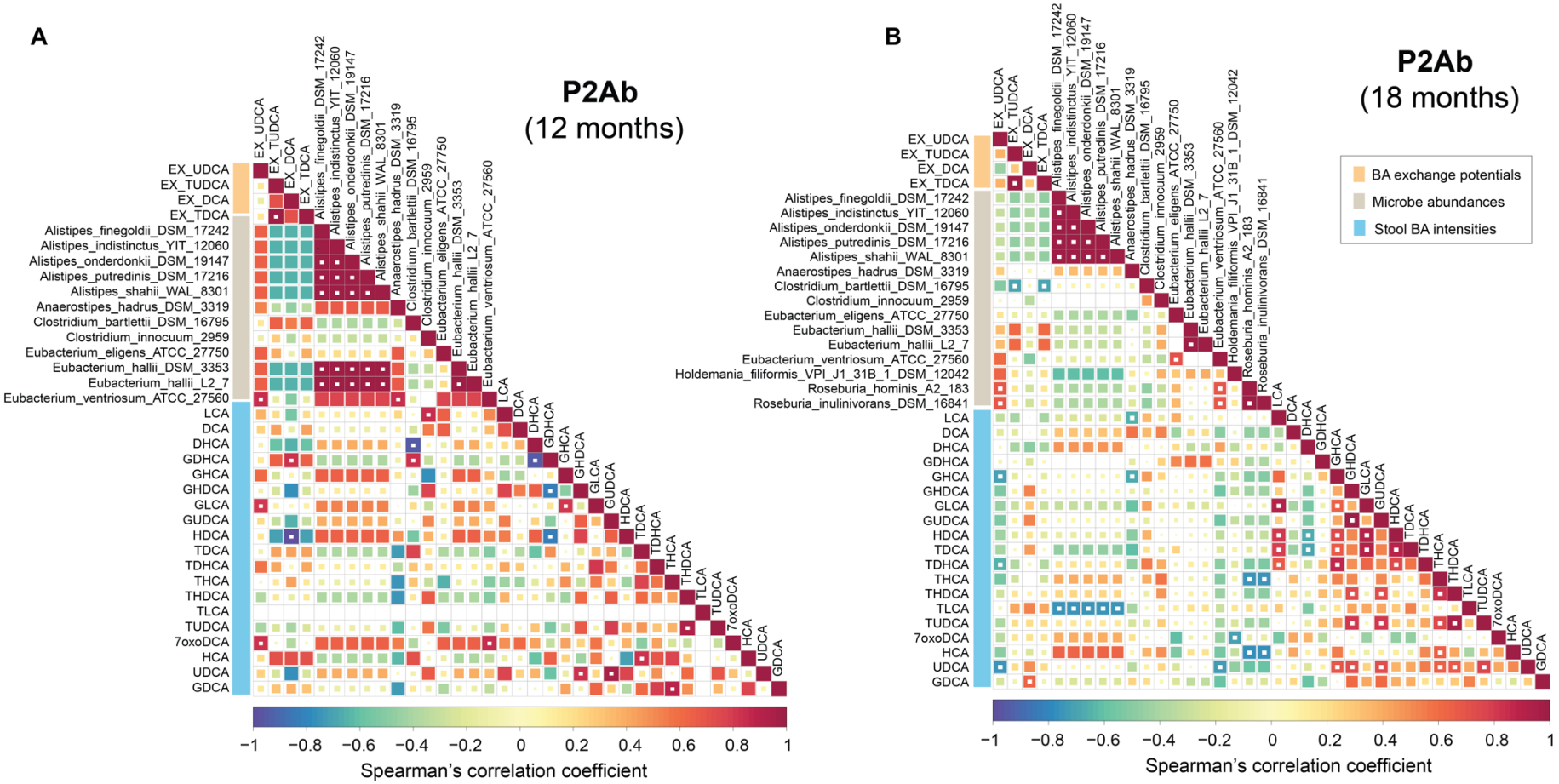
A
P2Ab
(12 months)
EX_UDCA
EX_TUDCA
EX_DCA
EX_TDCA
Alistipes_finegoldii_DSM_17242
Alistipes_indistinctus_YIT_12060
Alistipes_onderdonkii_DSM_19147
Alistipes_putredinis_DSM_17216
Alistipes_shahii_WAL_8301
Anaerostipes_hadrus_DSM_3319
Clostridium_bartlettii_DSM_16795
Clostridium_innocuum_2959
Eubacterium_eligens_ATCC_27750
Eubacterium_hallii_DSM_3353
Eubacterium_hallii_L2_7
Eubacterium_ventriosum_ATCC_27560
LCA
DCA
DHCA
GDHCA
GHCA
GHDCA
GLCA
GUDCA
HDCA
TDCA
TDHCA
THCA
THDCA
TLCA
TUDCA
7oxoDCA
HCA
UDCA
GDCA
−1 −0.8 −0.6 −0.4 −0.2 0 0.2 0.4 0.6 0.8 1
Spearman's correlation coefficient
B
P2Ab
(18 months)
BA exchange potentials
Microbe abundances
Stool BA intensities
Holdemania_filiformis_VPI_J1_31B_1_DSM_12042
Roseburia_hominis_A2_183
Roseburia_inulinivorans_DSM_16841
−1 −0.8 −0.6 −0.4 −0.2 0 0.2 0.4 0.6 0.8 1
Spearman's correlation coefficient

Supplementary Notes

Lamichhane *et al*.,

Figure S1. Factor analysis and identification of confounding factors affecting the microbiome. A density plot showing sample-wide distribution of (% of explained variances (EVs)) of various clinical and demographic factors associated with the normalized metagenomic analyzed in (n=111) stool samples.

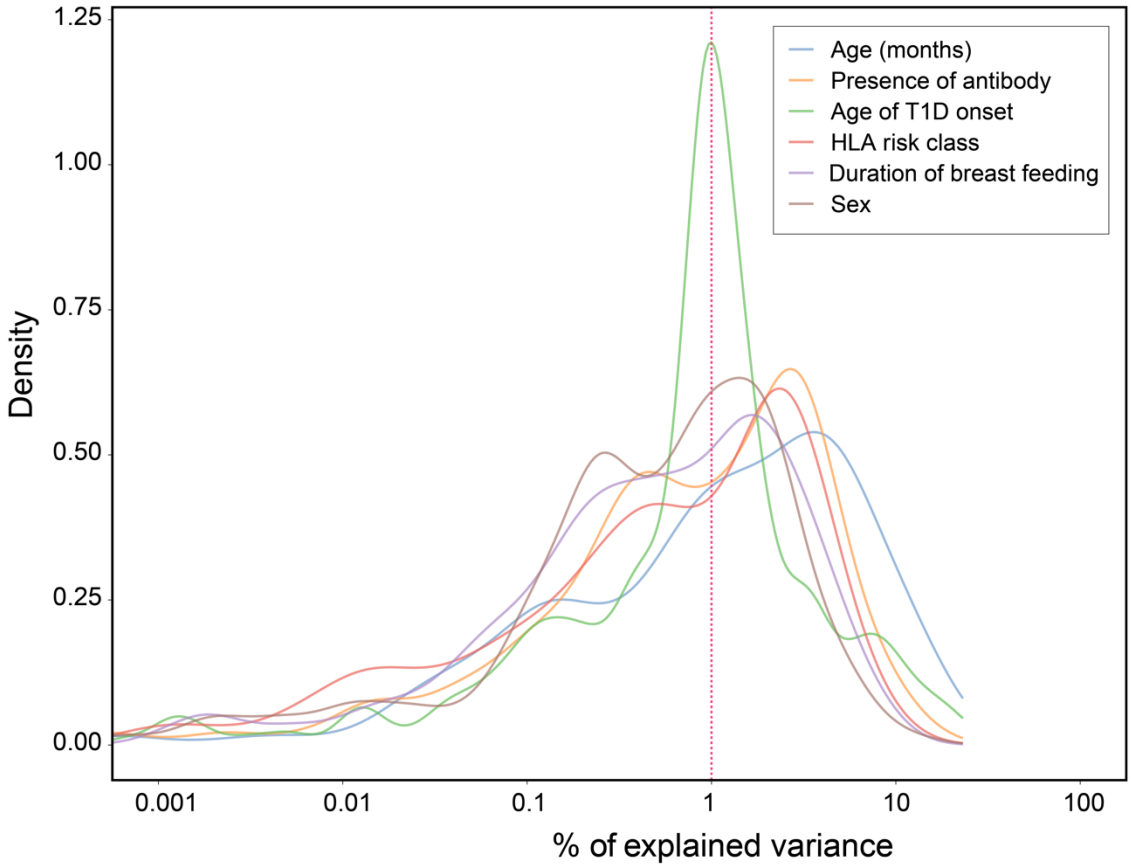

Figure S2. Modeling of pairwise interactions between 25 selected gut bacterial strains (*co-growth*) subjected. **(A)** The predicted relationship between all possible pairs of examined bacteria engaged in BA de-conjugation and BA biotransformation. *Amensalism*: In the paired simulation, one microbe grows slower than the other does, but their growth is not mutually dependent. *Parasitism*: One microbe grows faster than another does. *Competition*: In the paired simulation, both microbes exhibit slower growth as compared with their individual growth. *Neutralism*: Independent and unaffected growth of the microbes in the paired simulations. *Commensalism*: Growth of one microbe is faster and unaffected by the other. The definitions of mentioned concepts are derived from (Magnusdottir *et al.*, 2017). **(B)** Gut bacterial strain pairs that can biotransform BAs were grouped by their genus.

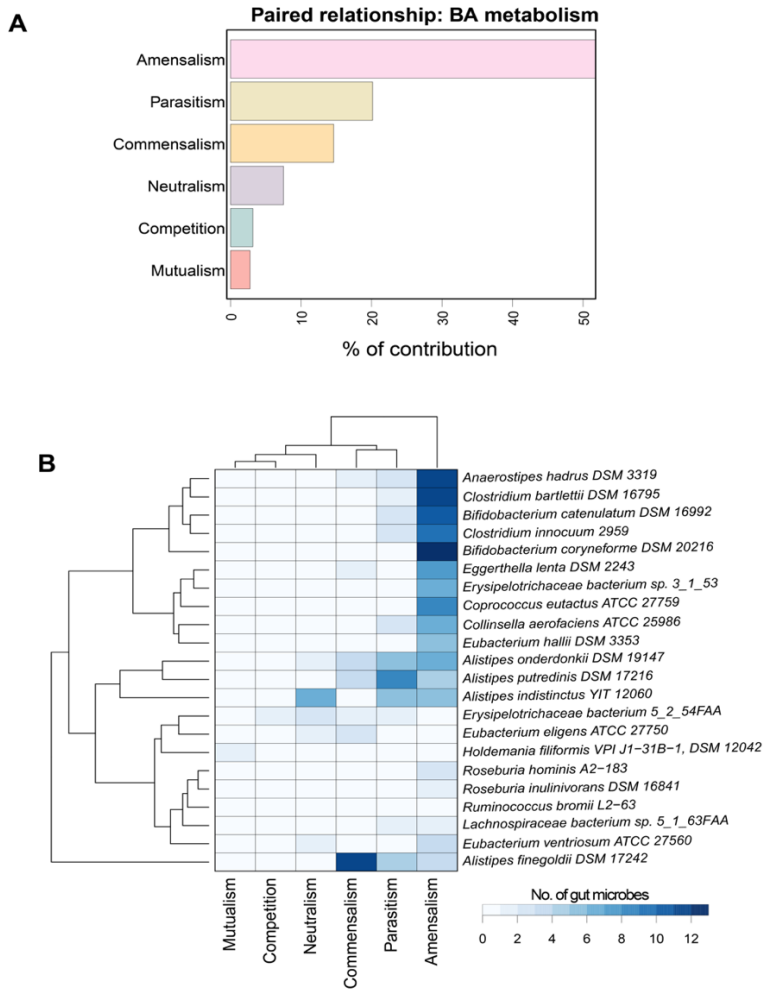

Figure S3. Bile acid reaction classes exhibited by the 25 abundant microbes. The BA reactions/pathways exhibited by human gut microbes spans between 10 different reaction classes that can carry out deconjugation, dehydrogenation, dehydroxylation and epimerization of BAs in the gut.

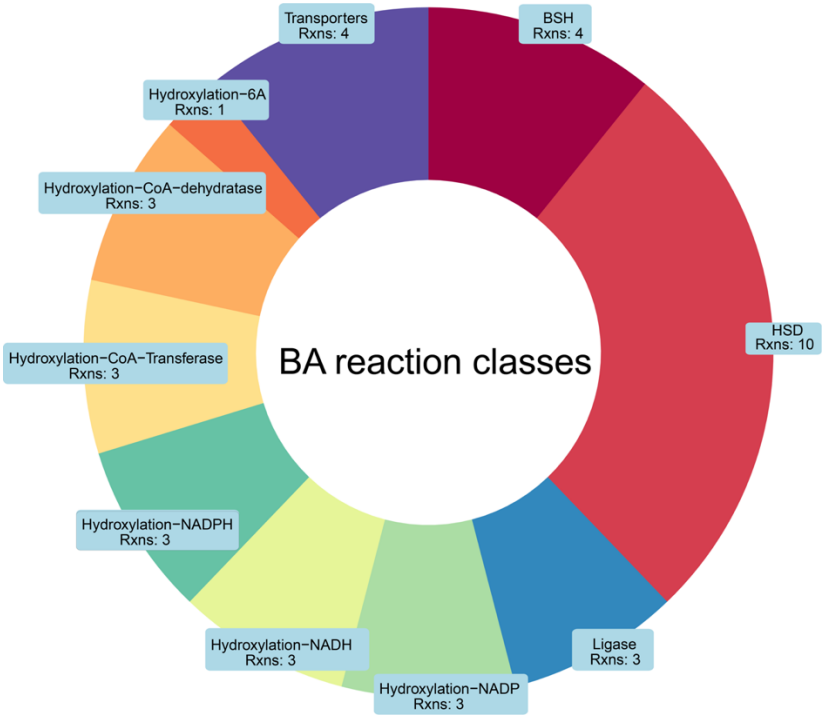

Table S1. Multivariate associations using linear models were performed with co-variates including age, sex, and case status (P2Ab or P1Ab or CTRs) in stool.

Metadata	Features	coefficient	P value	Q value
Age	LCA	1.765868	3.19E-35	3.95E-33
Age	HCA	-0.71767	1.96E-23	1.21E-21
Age	CA	-1.01563	2.19E-20	9.04E-19
Age	CDCA	-0.9442	3.85E-19	1.01E-17
Age	HDCA	1.017782	4.07E-19	1.01E-17
Age	GLCA	0.488118	5.37E-19	1.11E-17
Age	GDHCA	-0.18543	1.16E-15	2.05E-14
Age	TDCA	0.451116	1.21E-10	1.88E-09
Age	OXODCA	-0.58323	2.75E-10	3.79E-09
Age	UDCA	0.807496	1.29E-09	1.52E-08
Age	GUDCA	0.549565	1.35E-09	1.52E-08
Age	DCA	-0.5483	7.77E-09	8.03E-08
Age	THCA	-0.50224	8.87E-09	8.46E-08
Age	TaMCA	-0.64066	1.05E-08	9.29E-08
Age	GHDCA	0.531877	4.10E-08	3.39E-07
Age	bMCA	-0.5654	6.81E-08	5.28E-07
Age	TLCA	0.238253	5.38E-07	3.93E-06
Age	oxoHDCA	-0.42934	4.05E-05	0.000279
Age	GHCA	-0.1721	8.74E-05	0.00057
Age	TDHCA	-0.16553	0.000214	0.001328
Age	GCDCA	0.203357	0.001128	0.006658
Age	GDCA	0.203259	0.001189	0.006701
Age	aMCA	-0.1961	0.001382	0.007451
Case	GUDCA	-0.66431	0.009749	0.050371
Case	GHDCA	-0.6725	0.014903	0.073919
Case	TUDCA	-0.7258	0.026109	0.11991
Case	HDCA	-0.54519	0.028887	0.12793
Case	THDCA	-0.65175	0.044398	0.189841
sex	HDCA	-0.26414	0.017872	0.085236

Table S2. Multivariate associations using linear models were performed with co-variates including age, sex, and case status (P2Ab or P1Ab or CTRs) in serum.

Metadata	Feature	Coefficient	P value	Q value
Age	TDCA	0.810951	4.84E-34	5.61E-32
Age	HCA	-0.615	5.16E-29	2.99E-27
Age	GLCA	0.366212	3.35E-25	1.29E-23
Age	TaMCA	-0.66722	7.47E-21	2.17E-19
Age	GUDCA	0.692191	2.46E-18	5.72E-17
Age	THCA	-0.4358	5.13E-16	9.92E-15
Age	UDCA	0.584086	6.06E-15	1.00E-13
Age	GHDCA	0.650438	2.03E-13	2.95E-12
Age	X7oxoHDCA	-0.33823	3.78E-11	4.88E-10
Age	GDCA	0.992672	7.50E-11	8.70E-10
Age	TLCA	0.16878	9.46E-10	9.98E-09
Age	HDCA	0.503645	4.96E-09	4.79E-08
Age	X7OXODCA	-0.35812	6.31E-08	5.63E-07
Age	TCA	-0.38511	1.41E-07	1.17E-06
Age	TwMCA	0.239079	1.54E-07	1.19E-06
Age	TCDCA	-0.54483	3.05E-07	2.21E-06
Age	CDCA	-0.28592	8.93E-07	6.10E-06
Age	GHCA	-0.24791	1.23E-06	7.92E-06
Age	TUDCA	0.24461	1.94E-06	1.19E-05
Age	THDCA	0.235196	2.78E-06	1.61E-05
Age	wMCA	-0.06713	0.007594	0.040039
Case	HDCA	-0.5611	0.02448	0.118321
sex	TDHCA	0.019688	0.004911	0.027125
sex	GHCA	0.159941	0.013417	0.067668
sex	GCA	0.16621	0.034349	0.159378
sex	THCA	0.137237	0.04182	0.186583

Table S3 Multivariate associations using linear models were performed with co-variates including age, sex, and case status (P2Ab or P1Ab or CTRs) in the stool microbiome dataset.

Metadata	feature	coef	pval	qval
Age	t__GCF_000296465	0.004602	0.000156	0.07719
Age	t__GCF_000154465	0.007676	0.000153	0.07719
Age	t__Ruminococcus_gnavus_unclassified	-0.02405	0.000309	0.101766
Age	t__GCF_000311925	0.001811	0.000427	0.105464
Age	t__Bifidobacterium_breve_unclassified	-0.02191	0.000804	0.132415
Age	t__GCF_000190535	0.002788	0.000776	0.132415
Age	t__GCF_000146185	0.006975	0.00144	0.182298
Age	t__GCF_000469345	0.000243	0.00169	0.182298
Age	t__Veillonella_parvula_unclassified	-0.00865	0.001845	0.182298
Age	t__Escherichia_coli_unclassified	-0.01997	0.002691	0.221572
Age	t__Streptococcus_mitis_oralis_pneumoniae_unclassified	-9.06E-05	0.003431	0.260742
Age	t__GCF_000265365	0.002121	0.006453	0.455398
Age	t__Bacteroides_ovatus_unclassified	0.018325	0.011665	0.638927
Age	t__GCF_000153885	0.000159	0.012934	0.638927
Age	t__GCF_000209875	0.008028	0.012914	0.638927
Age	t__GCF_000468015	0.000374	0.011642	0.638927
Age	t__GCF_000185705	3.22E-05	0.010589	0.638927
Case	t__GCF_000159975	0.009565	0.001704	0.182298
Case	t__GCF_000157995	0.000447	0.002104	0.188982
Case	t__GCF_000218385	0.000305	0.010119	0.638927
Case	t__GCF_000190535	0.006662	0.021796	0.800568
Case	t__GCF_000242155	-0.00049	0.022627	0.800568
Case	t__GCF_000205025	0.00103	0.022923	0.800568
Case	t__Lactobacillus_ruminis_unclassified	0.002381	0.030614	0.800568
Case	t__Faecalibacterium_prausnitzii_unclassified	0.032737	0.035679	0.800568
Case	t__GCF_000239295	0.001043	0.037556	0.800568
Case	t__Bacteroides_ovatus_unclassified	0.042377	0.039878	0.800568
Case	t__GCF_000169035	-0.0067	0.042992	0.800568
Case	t__Streptococcus_parasanguinis_unclassified	0.000385	0.048034	0.800568
sex	t__Lactococcus_lactis_unclassified	0.000553	0.037624	0.800568
sex	t__Streptococcus_mitis_oralis_pneumoniae_unclassified	-6.30E-05	0.039398	0.800568
sex	t__Clostridium_symbiosum_unclassified	0.000892	0.046542	0.800568
sex	t__GCF_000157995	0.000111	0.047607	0.800568